MASTER

HVEM QUANTITATIVE STEREOSCOPY THROUGH THE FULL DAMAGE RANGE OF AN ION-BOMBARDED Fe-Ni-Cr ALLOY

S. Diamond   M. L. Bleiberg
I. M. Baron   R. Bajaj
R. W. Chickering

Westinghouse Advanced Reactors Division
Box 158, Madison, Pa. 15663

ABSTRACT

The swelling of a Ni-ion irradiated Fe-25%Ni-15%Cr alloy has been investigated employing high voltage (1 MeV) electron microscopy. Helium pre-injected samples were irradiated to a maximum dose of 92 dpa with 3.5 MeV $^{60}Ni^+$ ions at 600, 650, 700 and 750°C. By means of quantitative stereoscopy throughout the full range of ion damage, the void morphology, swelling and dislocation morphology as functions of the distance from the ion-entry surface of the foil were obtained. The dose also varied as a function of depth and, with this technique, swelling as a function of dose was determined from a single sample at each temperature. Swelling, void concentration, and void size varied with irradiation temperature with the maximum swelling of 7.4% occuring at 700°C. Several distinct dislocation configurations could be distinguished progressing inward from the ion-entry surface. The observations suggest that nucleation and growth of voids are related to dislocation densities and possibly to dislocation structure. The swelling-dose relationships were analyzed using a linear expression for each apparent swelling regime and the results interpreted in terms of the Brailsford and Bullough statistical rate theory. Two distinct steady-state swelling regimes exist at each irradiation temperature and the difference in the rates is attributed to the different kinetic development of the dislocation structure and densities in the two stages.

INTRODUCTION

The damage produced in metals and alloys by fast neutron fluences has been simulated in many experiments[1,2] by bombardment with high energy charged particles. The void formation, swelling, and irradiation-related

microstructural evolution during these particle bombardments occur a thousand fold more rapidly than during neutron exposure. This permits rapid detailed study of the damage process and of the possible mechanisms for the avoidance or suppression of swelling, which can have an important influence on the design and economics of the first wall for CTR.

The damage from charged particles occurs typically in a band within one or two microns of the ion-entry surface of the material. Since this thickness is too great to achieve an acceptable image resolution with conventional ($\lesssim$ 200 KeV) transmission electron microscopy, a sample has to be sectioned to a predetermined depth beneath the ion-entry surface and then backthinned to obtain regions thin enough for TEM. This requires several samples to measure the damage parameters throughout the full damage region and the depth of each sectioning is subject to considerable uncertainty. However, the thickness from which acceptable image resolution can be obtained with 1 MeV electrons is greater than the thickness of the damage region in materials of immediate interest for CTR and LMFBR applications, i.e. Fe-Ni-Cr alloys, which have been irradiated with Ni ions, (<5 MeV). By backthinning an ion-irradiated sample directly to the ion-entry surface, a section is obtained which includes the full damage range. High voltage electron microscopy (HVEM), quantitative stereo-scopy,[3] and associated computer codes[3] can then be used on a single sample to study the swelling, void concentration, and dislocation morphology through this range as functions of the distance from the ion-entry surface.[4] The dose also varies as a function of depth and, with this technique, swelling as a function of dose can be determined from a single sample.

This work reports such a full range HVEM study in an Fe-25%Ni-15%Cr alloy irradiated with $^{60}Ni^+$ ions to a maximum dose of 92 dpa at four irradiation temperatures. This alloy is a base for an experimental alloy series which was designed to obtain fundamental irradiation damage information for the development of new commercial alloys for use in reactors.

EXPERIMENTAL PROCEDURE

Pre- and Post-Bombardment Sample Preparation

The composition of the alloys used in this experiment is shown in Table 1. The alloy was fabricated by International Nickel Company by vacuum melting a 100 pound heat, extruding into 15.9 mm diameter bar stock, and cutting into 30.5 cm. lengths. The material was then swaged at room temperature to about 10.2 mm diameter, annealed at 1093°C for one hour in a H_2 atmosphere, centerless ground to 9.5 mm diameter, copper plated, and drawn into wire about 3.18 mm diameter. After the copper plating was removed from the wire, it was solution treated at 1150°C for 1 hour. Disc samples about 0.38 mm thick were cut for the ion bombardment experiment. The disc surfaces were prepared for bombardment using a multiple lapping technique. One face was ground on 600 grit abrasive. The discs were turned over and the second face (the ion-entry face) was lapped with successively finer diamond abrasive down to 0.1μ, resulting in a final sample thickness of ∿0.2 mm. Each lapping step was designed to remove all of the cold-worked surface material from the original cutting of the disc and from the previous lapping step. However, because of the extreme softness of this alloy, fine surface scratches were encountered even with these detailed lapping procedures; therefore, the surfaces to be bombarded were ion-milled, electropolished, and jetted over a 2mm. diameter in the foil center. The samples were then indium bonded to a copper plate and injected with 5 appm He to a depth of .025 mm. An additional 0.006 mm. was jetted from the sample surface to remove fine scratches which were observed after the He injection and demounting from the copper plate.

The samples were then mounted in tungsten alloy holders and irradiated with 3.5 MeV $^{60}Ni^+$ ions in the ANL Dynamitron at 600, 650, 700, and 750°C to a nominal peak of 90 displacements per atom (dpa). The peak dose rate was about 5×10^{-3} dpa per second.

After bombardment, a sample from each of the four irradiation conditions was demounted from its holder and prepared for HVEM examination by backthinning to the ion-entry surface.

3

Table 1. Composition Of Alloy, Wt. %

Fe	Cr	Ni	O	N	C	Co	Cu	Si	Mn
60.1	14.8	25.04	0.0154	0.0028	0.010	0.014	0.02	0.02	0.005

HVEM Technique

The irradiation-induced swelling in this alloy was measured using HVEM (on the U.S. Steel 1 MeV electron microscope) and stereomicroscopy techniques so that the entire damage range could be imaged simultaneously. This technique is summarized below.

A sample is first positioned in the HVEM in an appropriate orientation to produce the desired contrast conditions and a diffraction pattern and micrograph are recorded. The sample is then tilted through an angle of 6-9° along the selected Kikuchi band until a companion orientation with the desired contrast conditions is obtained. The diffraction pattern and micrograph in this orientation are then recorded. The two micrographs, constituting a stereo pair, are then mounted in an instrumented Hilger-Watts floating spot stereoscope and a magnified three-dimensional image of the irradiated sample is obtained. Void or precipitate coordinates along the entire damage range may be recorded on paper tape as transducer voltages from the instrumented stereoscope. The QUEST computer code is utilized to process these data and perform the following functions.

The program defines the surface plane of the foil with respect to an arbitrary origin by using the voltages corresponding to points on the foil surface. Next, the program calculates the perpendicular distance of defects from the foil surface and the defect sizes by using the voltages corresponding to two sides of each defect. From these computations the code calculates the following results:

1. Defect number density as a function of foil depth.
2. Size distribution at any foil depth.
3. Volume fraction of defects as a function of depth.
4. Swelling, in the case of voids, as a function of depth.
5. Maximum radius of defects.
6. Minimum radius defects.

4

7. Average defect radius.

These results are particularly useful in analyzing specimens which are ion bombarded. In such specimens, the number of displacements per atom varies as a function of depth. Therefore, the effects of radiation damage for a fixed irradiation time as a function of total displacements per atom can be determined from a single specimen.

This technique requires that a surface of the sample, such as the ion-entry surface, be observable in the stereo image so that a sufficient number of surface points may be recorded to define it mathematically and the perpendicular distance of the voids from that surface may be calculated.

In this experiment the sample surfaces, in general, were devoid of markings or stray contaminants such that they were rarely observable when the foil was imaged in absorption (void) contrast. However, when the foil was imaged in weak strain (dislocation-void) contrast, the intersection of dislocations with the surface provided a sufficient number of points to define the surface analytically. Therefore, the following procedure was used to analyze the swelling in the foil irradiated at 700°C:

A. Record two stereo pairs of a foil, one pair in absorption (void) contrast and the other in weak strain contrast.

B. Calculate the swelling in the stereo pair viewed in weak strain contrast.

C. Compare the swelling versus depth curve from this calculation to the calculated energy deposition curve.

The results obtained by this procedure are shown in Fig. 1 where the normalized swelling vs. depth is plotted for the case of weak strain contrast in which the foil surface position was measured. It can be seen that the peak in the swelling vs. depth curve occurs at ∿6700 Å, and is within ± 200 Å of the calculated peak in the energy deposition curve (dE/dx vs. x) calculated by the EDEP-1 Code.[5]

An alternative method was developed for approximately determining the surface plane from the measured void distribution. From the data for a stereo pair taken in absorption contrast in which the ion entry surface was

observable and had been experimentally determined, the equation of another plane was calculated by a least square method which minimized the sum of the squares of the vertical distances of the voids from this latter plane. This plane was shown to be parallel to the experimentally determined surface plane to within 5°. The swelling vs. depth dependence was found by an iterative process in which the plane determined from the void distribution was translated parallel to itself until the calculated peak swelling occurred at the peak in the energy deposition curve. The functional dependence of the swelling with depth calculated by the iterative method was shown to be the same as that calculated by the method utilizing the experimentally determined surface plane. Subsequently, for those samples where the surface plane was unobservable, the swelling vs. dose dependence was calculated by the iterative method.

Stereomicroscopic observations of the general microstructure were made not in optimum dislocation contrast, but at typical deviations of 4g to 8g such that the gross features of dislocation structure and void structure were simultaneously evident throughout the imaged range.

RESULTS

Microstructural Observations

Stereo examination of the HVEM micrographs in weak strain contrast established that four distinct dislocation configurations, although spatially mixed, could be distinguished at all temperatures:

1. A coarse dislocation structure within which the path of individual dislocation line segments could be followed over large distances.

2. Relatively large, well separated faulted loops randomly oriented.

3. Relatively large unfaulted loops, randomly oriented.

4. A densely tangled, fine dislocation network.

These four elements were the major components of the observed microstructure (in addition to voids), although occasionally small loops lying within larger loops were also observed.

6

In those regions where the dislocation network was the dominant feature of the microstructure, the void concentrations were higher than in the regions characterized by the coarse dislocation structure.

In the weak strain contrast imaging conditions, gross changes in dislocation densities and structure and void distribution as a function of depth into the foils were relatively easy to detect visually with the stereomicroscope. Although these observations were of a qualitative nature, they indicated that nucleation and growth of voids is related to dislocation densities and possibly to dislocation structures.

Fig. 2 summarizes schematically the dislocation and void structure observed at all four temperatures for this material. In all cases, two regions with different microstructures separated by a transition region were observed. The region nearest to the ion entry surface has been termed Region I and that farthest from the ion entry surface, Region II. The transition region was relatively sharp compared to the whole imaged range in which damage was observed. The dislocation structure in Region I appeared coarser and the voids were generally fewer and smaller than in Region II. Also, the voids in Region I seemed to decorate the dislocations. Since the minimum size of the voids was of the order of 100 $\overset{\circ}{A}$, the swelling in Region I cannot be attributed to any homogeneous or inhomogeneous incubation stage relating to void formation as is usually understood in nucleation.

SWELLING RESULTS

A micrograph of the typical void morphology observed in the irradiated samples is shown in Fig. 3. This is one-half of a stereo pair on which swelling measurements were made.

A plot of measured swelling as a function of depth below the ion-entry surface for each of the irradiation temperatures is shown in Fig. 4 along with the calculated energy deposition curve. The results of the stereo measurements are summarized in Table 2. It can be seen that the peak swelling increased, the void concentration decreased, and the void size increased with temperature up to 700°C. At 750°C the void

7

Table 2. Bombardment Conditions and Results
of Stereo-Measurements for Irradiated Fe-25Ni-15Cr Alloy

TEMPERATURE (°C)	PEAK DISPLACEMENT DOSE (dpa)	AVERAGE PEAK SWELLING (% $\Delta V/V_o$)	AT PEAK DOSE	
			AVERAGE VOID CONC. (per cm^3)	AVERAGE VOID DIAMETER (Å)
600 ± 15	86 ± 9	2.0	1.39×10^{15}	300
650 ± 15	83 ± 8	3.5	7.34×10^{14}	446
700 ± 20	90 ± 9	7.4	1.30×10^{14}	1003
750 ± 15	92 ± 9	0.6	1.42×10^{14}	433

concentration increased slightly but the void size was very much smaller
and the swelling was thus greatly diminished. The maximum swelling of
7.4% occurred at 700°C.

Since in Fig. 4 there appears to be a correlation between the spatial
distribution of the measureable damage in the form of swelling and the
energy per ion deposited within the material, it was assumed that there was
a statistical relationship between the measured swelling and the calculated
dose. Swelling vs. dose values were determined from the experimental
data for each temperature and are plotted in Fig. 5. It was further
assumed that, for these ion bombardments, the relationship between
swelling and dose was linear, similar to the swelling caused by neutron
irradiation where it has been assumed[6] that

$$\frac{\Delta V}{V_o} \% = S = R (F-F_{th}) \tag{1}$$

where F = the dose in displacements per atom (dpa)

   F_{th} = a "threshold" dose in dpa

   R = a steady-state swelling rate in % swelling/dpa

   S = the observed swelling in %.

A regression analysis was performed on the data to develop the
correlation between the swelling and the dose. The following are the
regression equations developed by this analysis:

8

600°C	Stage I	S = .0098 (F-32)	45 < F < 70	γ = .415	(2A)
	Stage II	S = .0874 (F-65)	70 < F < 90	γ = .95	(2B)
650°C	Stage I	S = .035 (F-45)	45 < F < 65	γ = .46	(3A)
	Stage II	S = .178 (F-64)	65 < F < 82	γ = .97	(3B)
700°C	Stage I	S = .0395 (F-35)	35 < F < 58	γ = .87	(4A)
	Stage II	S = .190 (F-51)	58 < F < 85	γ = .93	(4B)
750°C	Stage I	S = .007 (F-29)	30 < F < 70	γ = .82	(5A)
	Stage II	S = .0194 (F-62)	70 < F < 90	γ = .80	(5B)

where S is swelling and F is dose as in Eq. (1) and γ denotes the measure of statistical correlation.[7] In Fig. 5 both the data and the regression lines are plotted. The data points are labeled with A or B indicating different areas of the foil while 1 indicates a depth less than and 2 indicates a depth larger than that at which the peak occurs. For each irradiation temperature in Fig. 5 there can be seen two distinct linear portions of the swelling vs. dose plot. The portion characterized by the lower swelling rate is hereafter referred to as Stage I and the portion of higher swelling rate, Stage II.

Interpretation of the Data

Two distinct phases in the swelling process are consistent with these data at all temperatures. To analyze the nature of the processes contributing to each phase, some assumptions on the kinetic evolution of the microstructure are necessary.

The following fairly conventional picture regarding the nucleation of loops and voids was adopted. The first sign of radiation damage in this alloy is probably the nucleation of small interstitial and, possibly, vacancy loops. However, the rate of energy deposited into displacement processes (per unit distance per incoming particle) is larger deeper within the foil (Region II) than closer to the surface of the foil (Region I). Therefore, the number of loops nucleated (per unit volume) in region II would be expected to be larger than the number nucleated in region I and the mean distance between the loops in region II would be smaller than in Region I.

9

The second kinetic stage probably involves nucleation of small voids in the vicinity of dislocation loops, their stabilization by helium, and growth of both voids and loops in both regions. Since the mean distance between the loops is larger in Region I, they may be considered as growing independently without effects of competition between the loops being appreciable. The loops grow and their bias[8] approaches rather quickly the bias of straight dislocation line segments.

In Region II, however, due to the presence of a large number of small loops closely spaced, the interaction between loops soon becomes important, and with it, effects of competition among loops. This in general will have the effect of "slowing down" the growth of individual loops thus increasing the relative bias over and above the value expected for a straight edge dislocation.[8] Due to the higher loop density in Region II and the larger bias (as compared with Region I), nucleation of voids will be more probable and their growth rate enhanced as compared with Region I. The final stage of microstructural evolution probably involves stabilization of the dislocation structures first in Region II and later in Region I. Eventually a "fine" dislocation netowrk will develop in Region II and a "coarse" dislocation structure in Region I.

Analysis of Swelling-Dose Relationships

Our results, in particular Eqs. 2-5, may be interpreted at all temperatures within the framework of the approximate statistical rate theory of Brailsford and Bullough (B.B.).[9] The basic theory is summarized in the following equations.

$$\frac{\Delta V}{V_o} \% = S = \alpha K (t-t_o) F (\eta) \tag{6}$$

where

$$\eta = 400 \exp \ [- \frac{E_m^v}{K_B} (\frac{1}{T_s} - \frac{1}{T})] \tag{7}$$

$$F(\eta) = \frac{2}{\eta} [(1 + \eta)^{1/2} - 1 - \frac{\eta}{2} \exp \{- \frac{Q}{K_B} (\frac{1}{T} - \frac{1}{T_f})\}] \tag{8}$$

and for our case, with no precipitates,

10

$$\alpha = \rho_d \; 4\pi \; r_s \; C_s \; (\mathfrak{z}_I - \mathfrak{z}_V)/[(\rho_d + 4\pi \; r_s \; C_s)^2] \tag{9}$$

where: $\dfrac{\Delta V}{V_o} \% = S$ = swelling in percent

ρ_d = characteristic average dislocation line density

r_s = average void radius

C_s = average void density

$\mathfrak{z}_I - \mathfrak{z}_V$ = bias in percent

E_m^v = vacancy migration energy

k_B = Boltzman's constant

Q = activation energy for diffusion by the vacancy mechanism

T = temperature of irradiation in °K

T_s = temperature characteristic of the onset of measurable swelling

T_f = temperature characteristic of the termination of measurable swelling

K = displacement rate in dpa/sec

t = time in seconds

Kt_o = threshold dose

It is assumed that Eqs. 6-9 apply to each linear swelling regime which can be distinguished experimentally. Thus, the steady state swelling rate R appearing in Eqs. 2-5 may be thought of as being composed of two distinct factors:

$$R = \alpha \; F(\eta) \tag{10}$$

where α is a factor related to microstructure and defined by Eq. (9), and $F(\eta)$ is a phenomenological temperature dependent factor defined in Eq. (8). In practice, when a detailed numerical description of the kinetic evolution of the microstructure is not postulated, the parameters α, T_s and T_f are adjustable parameters, which are fixed for some given irradiation conditions. In Fig. 6, $F(\eta)$ is plotted as a function of temperature using the activation energy values recommended by B.B. for stainless steel

11

$(E_m^v = 1.4\text{eV}, Q = 3\text{eV})$ for several plausible choices of the parameters T_s and T_f.

If Eqs. (2-5) are compared with Eq. (6), the following interpretation is suggested. At each temperature there are two distinct stages in the swelling process, both corresponding to steady state swelling. The first stage corresponds to Region I with parameters $R_1(T) = \alpha_1 F(\eta)$ and threshold dose $F_{th}(1) = K t_o^{(1)}$, and the second stage corresponds to Region II with parameters $R_2(T) = \alpha_2 F(\eta)$ and threshold dose $F_{th}(2) = K t_o^{(2)}$.

Microstructural observations and the dynamic picture outlined above suggest that the threshold doses as well as the two steady state rates at each temperature are associated with the dynamic evolution of the dislocation structure in Regions I and II. In other words, the difference in swelling rates R_1 and R_2 at the same temperature is a reflection of the fact that the dynamic evolution of the microstructure is different in Regions I and II. The functional dependence in Eq. (9) substantiates this observation.

Let us assume for the moment, as a working hypothesis, that Eq. (9) holds in some average sense for Stage II uniformly, i.e., independent of temperature over the range investigated here. Thus, the change in swelling rates between different temperatures in Stage II is viewed as being due solely to the temperature variation of the phenomenological factor $F(\eta)$. A similar assumption is made for Stage I.

If we then plot the experimentally measured rate in Stage I and Stage II as a function of temperature in Fig. 7, we note that the two curves have very similar temperature dependence. The form of the temperature dependence is characteristic of steady state swelling in both stages, which is a self-consistent check on our original assumption of steady state swelling in both stages. Furthermore, if we compare Fig. 7 with $F(\eta)$ (Fig. 6) the following result is found. Of all the functions $F(\eta)$ there are several which are consistent overall with both curves in Fig. 7. For example, if we base our comparison on the curve $F(\eta)$ with $T_s = 773°K$, $T_f = 1035°K$ (Fig. 6), which corresponds approximately to onset

12

of measurable swelling at 500°C and termination at 762°C (which is consistent with the experimental data), the following average values are retrieved for α:

$$\alpha_1 = \alpha(\text{Stage I}) = 1/11.39 = .09 \tag{11}$$

$$\alpha_2 = \alpha(\text{Stage II}) = 1/2.37 = .42 \tag{12}$$

If this theoretical curve $F(\eta)$ is accepted with the above parameters, we may iterate on our working hypothesis (that α_1 and α_2 are temperature independent) and allow the factor α to vary with temperature. Thus better agreement between theory and experiment may be obtained. Thus refined estimates based on $F(\eta)$ with $T_s = 773$ and $T_f = 1035$ are:

Stage I	Stage II
α_1 (750°C) = .23	α_2 (750°C) = .70
α_1 (700°C) = .09	α_2 (700°C) = .42
α_1 (650°C) = .09	α_2 (650°C) = .42
α_1 (600°C) = .03	α_2 (600°C) = .32

These results may now be used in conjunction with Eq. (9) to get a lower bound for the <u>average</u> bias parameters characterizing the dislocation structure at each temperature for each stage. This can be done by noting that in Eq. (9) the factor containing the average dislocation densities, void radii, and void concentrations is bounded by the numerical factor 0.25. Thus for each steady state swelling regime at each temperature we have

$$\alpha_{1,2}(T) < .25 (z_I - z_v) \quad \text{or} \quad (z_I - z_v) > 4\,\alpha_{1,2}(T) \tag{13}$$

Thus for Stage I

$$(z_I - z_v) > .92\% \text{ at } 750°C$$
$$(z_I - z_v) > .36\% \text{ at } 700°C$$
$$(z_I - z_v) > .36\% \text{ at } 650°C$$
$$(z_I - z_v) > .12\% \text{ at } 600°C$$

and for Stage II

$$(z_I - z_v) > 2.80\% \text{ at } 750°C$$
$$(z_I - z_v) > 1.68\% \text{ at } 700°C$$

13

$$(z_I - z_v) > 1.68\% \text{ at } 650°C$$
$$(z_I - z_v) > 1.28\% \text{ at } 600°C$$

Note that the average bias parameters in Stage II are consistently lower bounded by larger numbers at each temperature than the average bias parameters corresponding to Stage I. Slightly different lower bounds on the bias would be calculated if the analysis is based on $F(\eta)$ with different T_s and T_f but the relationship between Stage I and Stage II remains invariant.

This may be taken as an indication of the different kinetics underlying the development of the dislocation structure in Stage I and Stage II.

These results may have major implications in the comparison of charged particle bombardments between various investigations, in the comparison of simulation data with neutron data, and in the comparison of neutron data obtained from different reactors. This work has shown that the swelling rate of Fe-25Ni-15Cr was increased by a factor of five by the change in microstructure between Stage I and Stage II. Thus, comparison of swelling results without a simultaneous comparison of microstructures is of little value. If an equivalent dose value is used, it must be equated with an equivalent microstructure. It would be expected that a "saturation" microstructure would evolve under all bombarding particles at which point swelling rates could be compared. This investigation indicates that high doses ($\geq$ 70 dpa) are required to achieve this microstructure in fully annealed simple ternary Fe-Ni-Cr alloys.

CONCLUSIONS

1. An Fe-25%Ni-15%Cr alloy, Ni-ion bombarded at 4 temperatures to 90 dpa and examined by full range HVEM stereoscopy, showed maximum swelling of 7.4% at 700°C.

2. A bi-linear swelling-dose relationship appears to hold over the entire temperature range investigated.

3. The experimental results can be interpreted at all temperatures using the B.B. statistical rate theory approach to swelling in irradiated materials.

4. Application of the B.B. model indicates that the difference in the swelling rates in the two distinct swelling regimes at each temperature is the result of the different kinetic development of the dislocation structure and densities in the two stages.

ACKNOWLEDGEMENTS

REFERENCES

1. R. S. Nelson, J. A. Hudson, D. J. Mazey, G. P. Walters and T. M. Williams, 430; G. L. Kulcinski, J. L. Brimhall, and H. E. Kissinger, 449; J. S. Armijo and T. Lauritzen, 479; A. Taylor and S. G. McDonald, 499; D. W. Keefer, A. G. Pard, and D. Kramer, 511; in Radiation Induced Voids in Metals, J. W. Corbett and L. C. Ianniello, Eds., U. S. Atomic Energy Commission Office of Information Service, Washington D. C., 1972.

2. W. G. Johnston, J. H. Rosolowski, A. M. Turkalo, and T. Lauritzen, Journal of Nuclear Materials, 47, 155 (1973).

3. L. E. Thomas and S. Lentz, in Proceedings of the 32nd Annual Electron Microscope Society Meeting, St. Louis, Mo., 1974.

4. A. F. Rowcliffe, S. Diamond, M. L. Bleiberg, J. Spitznagel, and
    W. J. Choyke, in ASTM Symposium on The Effects of Radiation on
    Structural Materials, Gatlinburg, Tenn., June 1974, in press.

5. I. Manning and G. P. Muller, Computer Physics Communications, 7,
    85, 1974.

6. J. I. Bramman, K. Q. Bagley, C. Cawthorne, E. J. Fulton, and
    W. D. J. Sinclair, in Voids Formed by Irradiation of Reactor
    Materials, S. F. Pugh, Ed., Proceedings of the British Nuclear
    Energy Society, London, 27, (1971).

7. W. Feller, An Introduction to Probability and Its Application,
    J. Wiley & Sons, New York, N. Y., Vol. 1, 221 (1950).

8. W. G. Wolfer, M. Ashkin, J. P. Foster, A. Biancheria, and A. Boltax
    in ASTM Symposium on The Effects of Radiation on Structural
    Materials, Gatlinburg, Tenn., June 1974, in press.

9. A. D. Brailsford and R. Bullough, Journal of Nuclear Materials,
    44, 121, (1972).

FIGURE LIST

Figure 1. Energy Deposition Curve and Normalized Swelling Curve for Voids Imaged in Void and Dislocation Contrast where Dislocation Intersections with Foil Surface Define the Surface
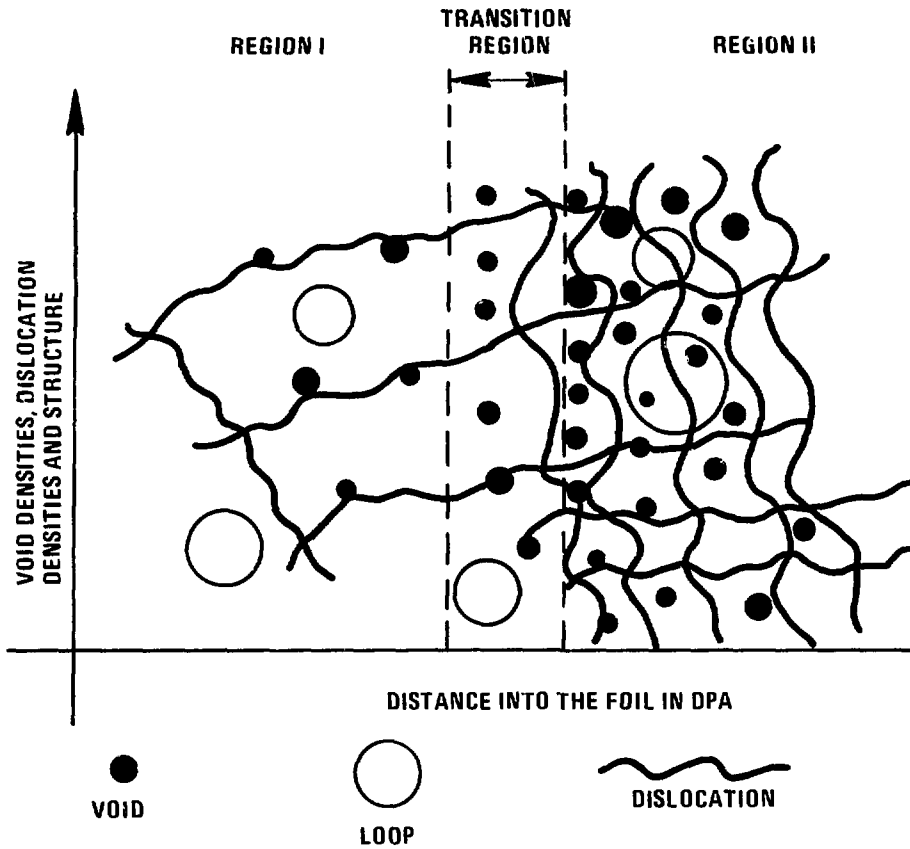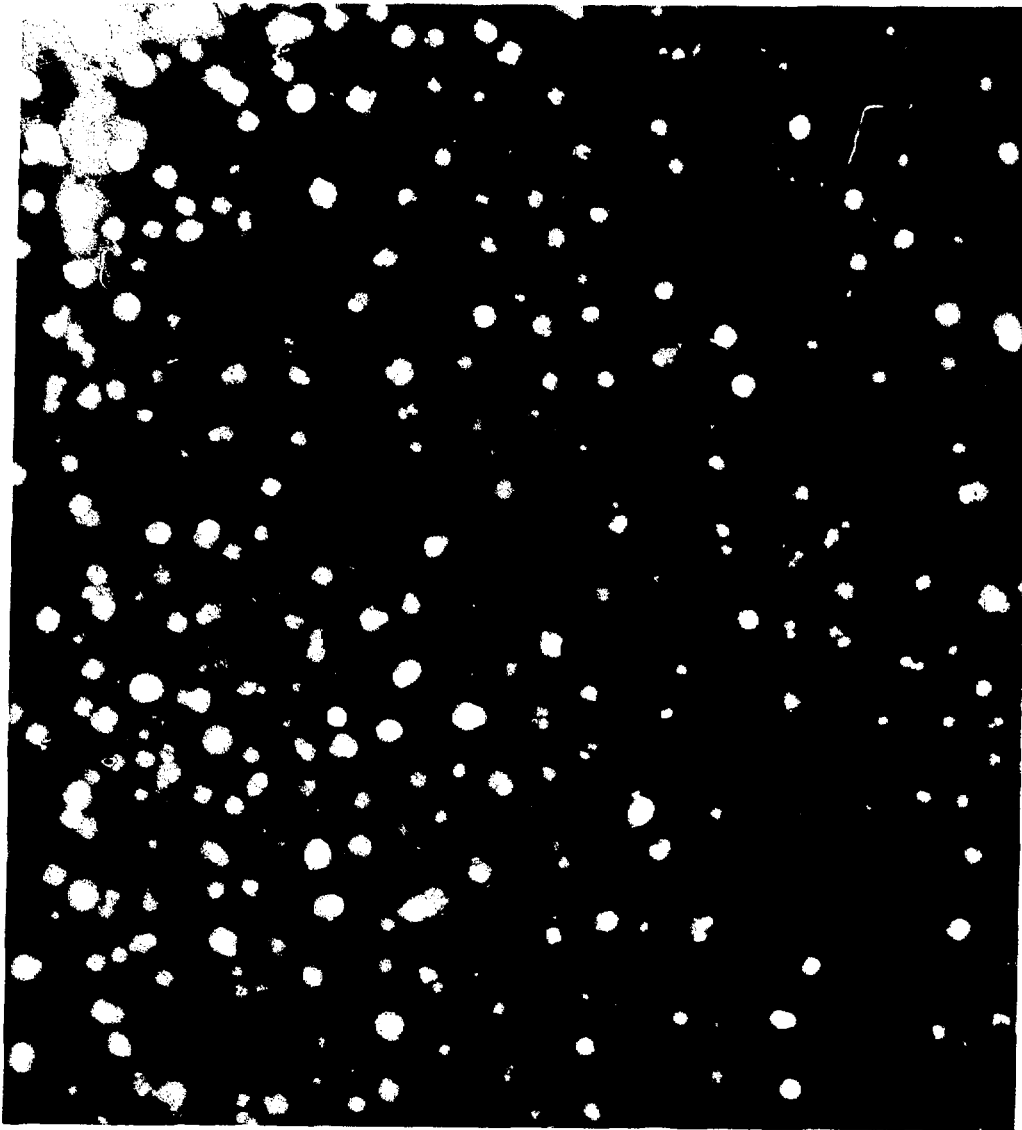
8192-1

Figure 2. Schematic Illustration of the Microstructural Features of Region I and Region II in Nickel Ion Bombarded Fe-25%Ni-15%Cr

8192-2

0.5μ

51936

Figure 3. Voids in Fe-25%Ni-15%Cr Alloy, Bombarded with 3.5 MeV Ni$^+$ at 700°C, Dose 90 dpa; 1 MeV Electron Micrograph $Z \sim |001|$, Bright field |200| Systematic s_{8g} 0

8192-3
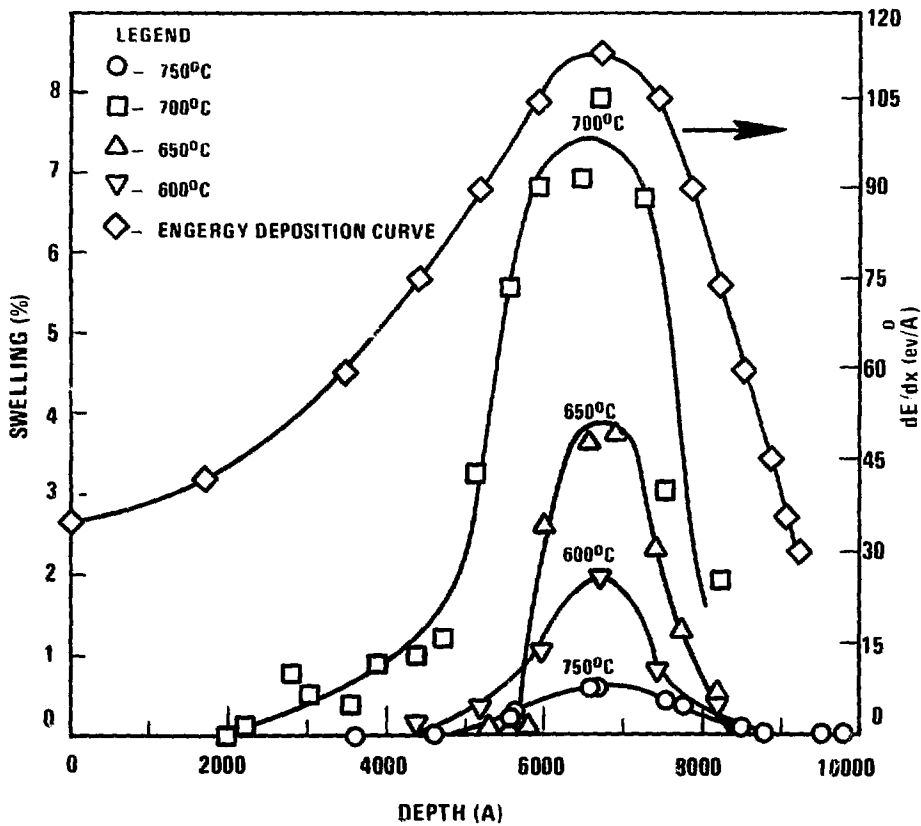
Figure 4. Swelling vs Depth Curves And Energy Deposition Curve For Fe-25%Ni-15%Cr Alloy Bombarded With 3.5 MeV ^{60}Ni$^+$ At 600, 650, 700, 750°C.
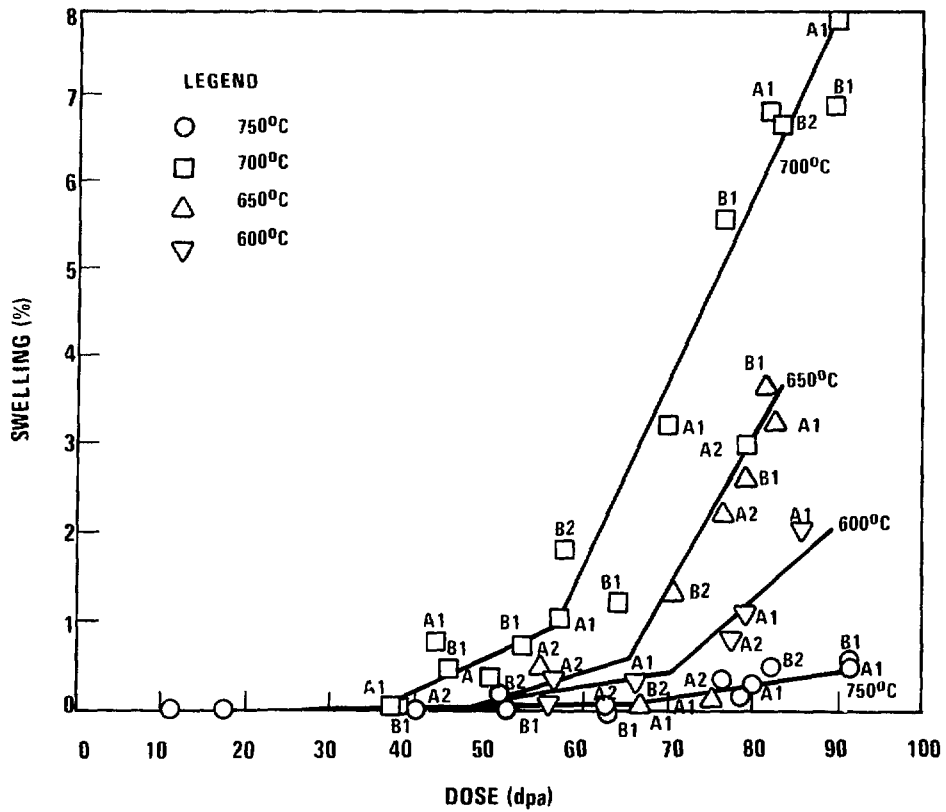
8192-4

Figure 5. Swelling As A Function Of Dose And Temperature For
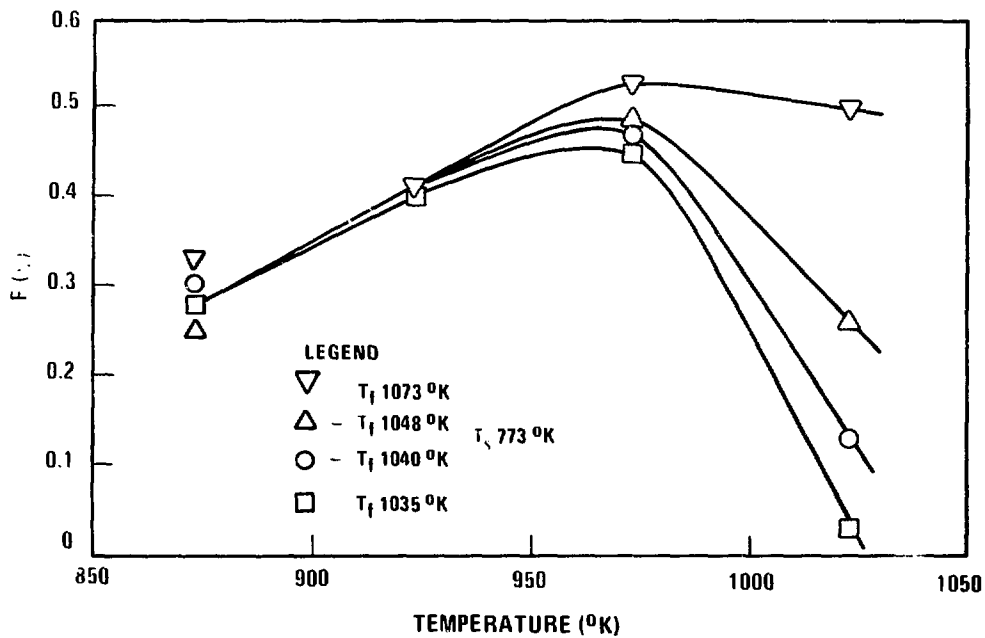Fe-25%Ni-15%Cr Alloy.

8192-5

Figure 6. F As A Function Of Temperature With T_f And T_s As
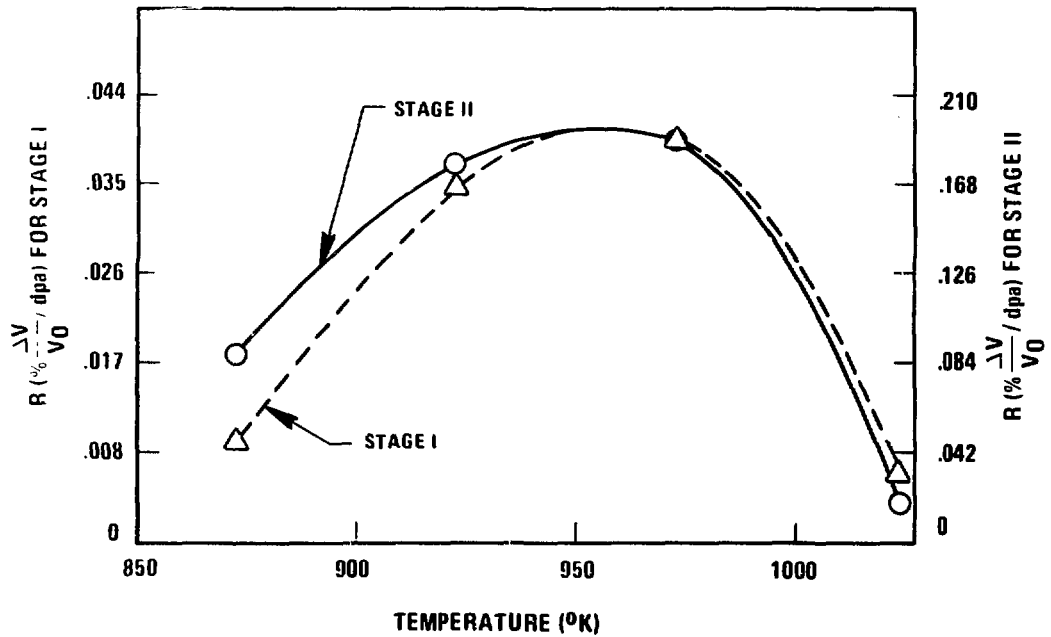Indicated; $E_v^m = 1.4$ eV, $Q = 3$ eV.

8192-6

Figure 7. Experimentally Measured Swelling Rate As A Function Of Temperature For State I And Stage II.

8192-7